

Elsevier Editorial System(tm) for High Energy Density Physics
Manuscript Draft

Manuscript Number:

Title: Ultra-Intense Gamma-Rays Created Using the Texas Petawatt Laser

Article Type: Research Paper

Keywords: Gamma Rays, Petawatt Lasers, Laser-Solid Interactions

Corresponding Author: Mr. Alexander Henderson,

Corresponding Author's Institution: Rice University

First Author: Alexander Henderson

Order of Authors: Alexander Henderson; Edison Llang; Nathan Riley; Pablo Yepes

Ultra-Intense Gamma-Rays Created Using the Texas Petawatt Laser

Keywords: Gamma Rays, Petawatt Lasers, Laser-Solid Interactions

Abstract:

In a series of experiments at the Texas Petawatt Laser (TPW) in Austin, TX, we have used attenuation spectrometers, dosimeters, and a new Forward Compton Electron Spectrometer (FCES) to measure and characterize the angular distribution, fluence, and energy spectrum of the X-rays and gamma rays produced by the TPW striking multi-millimeter thick gold targets. Our results represent the first such measurements at laser intensities $> 10^{21} \text{ W*cm}^{-2}$ and pulse durations $< 150 \text{ fs}$. We obtain a maximum yield of X-ray and gamma ray energy with respect to laser energy of 4% and a mean yield of 2%. We further obtain a Full Width Half Maximum (FWHM) of the gamma distribution of 37° . We were able to characterize the gamma-ray spectrum from 3 MeV to 90 MeV using a Forward Compton Electron Spectrometer, with an energy resolution of 0.5 MeV and mean kT of $\sim 6 \text{ MeV}$. We were able to characterize the spectrum from 1 to 7 MeV using a Filter Stack Spectrometer, measuring a mean gamma-ray temperature for the spectrum from 3 to 7 MeV of 2.1 MeV.

I: Introduction

When a laser of intensity greater than a few times 10^{18} W/cm^2 strikes a solid, high-Z target it couples a significant fraction of its energy to hot electrons with kinetic energy $> m_e c^2$. [1,2, 3,4] In a dense, high-Z, conductive material such as gold, a significant fraction of these electrons will undergo bremsstrahlung, producing copious gamma and x-rays. See Gibbon 2005 [5] for a review of this topic. The development in recent years of petawatt-class lasers such as the Texas Petawatt Laser (TPW) in Austin, TX opens up new potential for producing and studying ultra-intense, short-pulse multi-MeV gamma rays.

In petawatt class lasers, as much as 50% of the laser energy can be converted to hot electrons [6]. In principle, based on our Monte Carlo simulations, 30-50% of hot electron energy is convertible to gamma-rays, for a total laser to gamma-ray conversion factor of 15-25%, far in excess of any other mechanism. We measure a maximum efficiency of laser energy to gamma rays of 4% and a mean conversion efficiency of 2%. This would result in a lower laser energy to hot electron energy conversion rate of about 5-15%. The total laser-energy-to-gamma-ray conversion efficiency we obtain is short of the

theoretical maximum but still high enough to be promising.

Intense gamma-ray beams have potential novel applications for experimental physics and new technologies. For instance, colliding intense gamma-ray beams can potentially create a pure pair plasma via (γ, γ) pair production if the gamma-ray fluence is above a certain threshold. [7] For other pair-production mechanisms such as Trident and Bethe-Heitler [7], the e^+/e^- ratio is far short of a true pair plasma [8]. Such gamma-ray beams may also be useful for interrogating material hidden inside shielded containers, i.e. detecting concealed nuclear materials, and for nuclear medicine.

In the process of attempting to measure and characterize the gamma-ray beams produced by the interaction of petawatt class lasers with high-Z solid targets, we have also applied a method of gamma-ray spectrum measurement using Compton scattering, as suggested by Ahrens et al.[9] in 1972, developed by Matscheko and Ribberfors[10] and Morgan et al. [11], and more recently used by such groups as Reims et al. [12]. Following the example of Morgan et al. [11], we have chosen to consider Compton electrons scattered near 0 degrees. Then, we measure a wide range of Compton electron energies and adjust the acceptance angle and the thickness and type of converter material in order to sample different energy ranges. We refer to this method hereafter as Forward Compton Electron Spectroscopy (FCES). We measured the energy of the electrons using a rare earth permanent magnet with peak field strength of about 0.6 Gauss which had previously been modeled using GEANT4 Monte Carlo simulation [13, 14] based on a measured field map and calibrated by using mono-energetic electron beams from a linear accelerator. We refer to this device hereafter as a Forward Compton Electron Spectrometer (FCES). In our experiments, we achieved good results with a combination plastic and copper converter and with Compton electrons accepted into a $\sim 5^\circ$ angle, with the deconvolved spectrum matching Monte Carlo models between 3 and 50 MeV.

As in the method proposed by Morgan et al. [11] and Reims et al. [12], this method of measuring gamma ray spectra using Compton scattering and permanent magnets is compact, light, and simple enough that it could potentially be deployed to measure the energy spectrum of high-energy medical x-ray lines with greater ease and efficiency than the methods commonly used today [12].

II: Experimental Set-up

Experiments were carried out at the TPW located in Austin, TX in Target Chamber 1 (TC1) for high-intensity shots with an $f/3$ dielectric parabolic mirror donated by Los Alamos National Lab using gold targets. The cylindrical targets had thicknesses from 0.2 mm to 1 cm and diameters from 2 mm to 4.5 mm. The angle between target normal and laser forward was varied between 25 degrees and 45 degrees. The laser and target parameters are listed in Table 1.

Magnetic spectrometers were used to measure the electron and positron spectra as well as proton spectra from back-surface contaminants. In addition, two Filter Stack (or attenuation) Spectrometers (FSS) (see Section IV) were employed to measure the low-energy gamma ray spectrum, and a FCES was used on some runs to measure the gamma spectrum at higher energies (Section V). The full layout of TC1 is shown in figure 1.

The measured emergent electron spectrum for a 1 mm target (Fig. 2) was used as the hot electron spectrum for the Geant4 Monte-Carlo simulation used throughout this paper. [13,14] The measured spectrum has excess attenuation at lower energies compared to the true incident spectrum, but for energies above 1.5 MeV this should not be significant. The angular distribution of incident electrons was assumed to be a Gaussian with a Full Width, Half Maximum (FWHM) of 20 degrees. This was based on the work of Chen et al. [15b] and is consistent with the results of Dosimeter measurements of gamma and x-rays produced by the electrons (Section VI). The time profile was assumed to be a Gaussian with a FWHM of 150 fs, the duration of the main pulse of the TPW.

Section III: Filter Stack Spectrometer Results:

Two filter stack X-ray spectrometers were used to characterize the Bremsstrahlung spectrum, based on work by C. D. Chen et al.[16] Due to the high X-ray fluence produced at the target, the spectrometer design chosen relies on differential filtering with high-Z absorbers. The detector media are image plates, which are removed and read out after every shot. Figure 3 shows a diagram of one of these spectrometers. Seven channels are read out directly, and numerical deconvolution is used to produce the recorded energy spectrum. Measured data is recorded as photostimulated luminescence (PSL), proportional to deposited photon energy. This proportionality is effectively linear over the energy range of interest.

In order to deconvolve the spectra, the detector response is modeled numerically using the FLUKA particle transport

code.[17, 18] A sequence of ten monoenergetic photon beams per energy decade was propagated through the filter stack, and the resulting energy deposited in the image plate layers was recorded. The output spectrum is calculated using the GRAVEL code, which uses a modification of the SAND-II regularized nonlinear least squares algorithm.[19, 20] The resulting output spectrum was binned in regions corresponding to the monoenergetic response function inputs.

To calibrate this instrument we used an X-ray beam line with a known spectrum at the Mary Bird Perkins Cancer Center (MBPCC) in Baton Rouge, Louisiana. In figure 4, we can see that the deconvolved FSS spectrum agrees with the input X-ray spectrum within 30% between 1 and 2.5 MeV, and within 10% between 3 and 5 MeV. We may thus compare the FSS results on TPW experiments with simulation results in the range of 1 to 5 MeV.

Figure 5 shows results from the TPW experiments using the FSS and comparisons with our Geant4 Monte Carlo simulation. We compare the Monte Carlo spectrum obtained from our hot electron spectrum passing through different Au target thicknesses with the results of the FSS for that target and achieve a good match, considering the accuracies mentioned above, with the exception of an occasional “bump” between 1 and 3 MeV that is likely due to artificial numerical effects in the in the unfolding algorithm.

From the exponential “tail” of the FSS spectrum in a log-linear plot (Figure 6 a-b) we obtain effective temperatures (kT) of about 1.6 to 2.9 MeV for the Gamma ray distribution, with a mean of 2.1 MeV. The hot input electrons had a temperature of about 16 MeV, so we suspect that in this energy range (3 -7 MeV), bremsstrahlung gamma rays from secondary electrons dominate over those from primary electrons. Figure 6c shows an overlay of GEANT4 Monte-Carlo simulation results showing a temperature of around 2.5 MeV, within the measured range. In Figure 6d we see that the low energy gamma ray temperature is inversely correlated with laser energy, but in Figure 6e shows that this temperature is flat with laser intensity.

Section IV: Forward Compton Electron Spectrometer Results

The gamma ray spectrum with energies greater than a few MeV cannot be measured effectively using the FSS due to the energy-independence of the attenuation coefficient. Yet the short pulse nature of the TPW-produced gamma rays also cannot be measured using single-photon counting detectors such as scintillators. Hence we decided to employ a technique suggested by Morgan et al. [10]. When gamma-rays hit a low-Z thin target, the Compton scattered electrons in the forward

direction (near 0°) have an energy which correlates simply with the the generating gamma ray through the Compton scattering formula in the small angle approximation about 180° [21]:

$$\lambda' - \lambda = \frac{h}{m_e c} \left(2 - \frac{\theta^2}{2} \right)$$

where θ is the angle of the electron from photon incidence, or alternately the deviation of the scattered photon from 180° from photon incidence.

The idea, then, is to use these forward Compton scattered electrons to measure the high-energy gamma ray spectrum by narrowly collimating both the incident gamma-rays and scattered electrons.

For our FCES (Fig. 7), we use a magnetic electron spectrometer which consists of image plates on both sides of a gap between rare earth magnets. We then attached a Compton scatterer, consisting of varying combinations of polyethylene, aluminum, copper, and tin plates. In front of this we inserted a narrow collimator made of copper and lead totaling over 10 cm with a 6 mm diameter hole to collimate gamma rays. The FCES is placed nearly flush with an external glass porthole of TC1 (Fig. 1) at a distance of approximately 1 m from the target, so that the incident gamma ray beam is $< 1^\circ$ from the converter normal direction. The acceptance angle of Compton electrons was varied by means of teflon blocks with 6 mm diameter holes in them, so that the acceptance angle could be varied from 25° to 4.5° . The image plates were placed on both sides of the magnet gap to catch both positrons, electrons, and scattered x-rays, thus providing a way to subtract out external background and pair creation electrons, which compete with Compton electrons for thick converters.

In order to properly deconvolve the FCES plate images, we simulate the predicted Compton electron spectrum using GEANT4. In this simulation, we shoot a large number of gamma rays at fixed energy increments, e.g, 10000 at 0.5 MeV, 10000 at 1.0 MeV, etc. The resulting point-spread function (psf) can be inverted to obtain the original gamma ray distribution given the distribution of Compton and pair-produced electrons. While this specific simulation was not directly validated, similar simulations have been validated for the production of gamma rays (see section III above), as well as positrons and electrons under different conditions [22, 23].

Next, we constructed a detector response matrix (DRM) of the gamma-ray-to-Compton-electron process and used a previously developed psf [22] for the electron-to-image-plate signal to deconvolve the image plate results into a gamma-ray spectrum. These psfs were constructed by simulating a large number (10^3) of particles injected at fixed energies in 0.5 MeV intervals and using Matlab to obtain a pseudo-inverse of the resulting matrix. In order to remove as much noise and non-Compton electron background as possible, first the images are separated into a “background” region, and a “signal” region.

Then, the signal level on each image is integrated along the y-axis and the background level determined by subtracting the positron image. Then, the averaged value of the background regions is subtracted from each corresponding point in the signal region along the direction of changing energy. See Figure 8 for a flow-chart of the process.

Figure 9 show sample results of deconvolving the spectra for several shots of 1 mm thick gold targets. The electron spectrometer was limited to electron energies ≤ 50 MeV, so gamma rays ≥ 50 MeV could not be measured. The region below 1.3 MeV is similarly affected. In addition, electron energy such that the mean free path (mfp) is less than the thickness of the converter (7 mm) is 10 MeV for tin and 7 MeV for copper, so emergent scattered Compton electrons whose energy is less than these energies provide only a partial sampling of gamma rays below those energies. We compare the remaining region with simulation. We find that for a converter consisting of 12.5 mm of plastic and 7 mm of copper we are able to accurately characterize the gamma-ray spectrum from 3 MeV to 90 MeV, with an energy resolution of 0.5 – 1.5 MeV, depending on the energy range. Ahren et al [9] proposed a detector on a similar principle to measure up to 300 MeV with a resolution of 20 keV at 22 MeV. Matschekot and Ribberfors produced a Compton spectrometer using thin lucite, a material with a much lower Z-value and density than we used, that functioned at 20-200 keV with a resolution of 0.42 keV. [10] We intend to improve our resolution by using Monte Carlo simulation to carefully model the conversion process and by improving our background subtraction algorithm.

From the exponential tail of the spectrum, an effective temperature (kT) may be determined. From our TPW data, we obtain a mean temperature of 6.6 MeV. Note that this is significantly higher than the 2.1 MeV mean temperature seen using the FSS spectrometer, supporting the conclusion in section IV that the FSS spectrum was dominated by bremsstrahlung from secondary electrons. Figure 9d shows the GEANT4 Monte-Carlo simulation for the gamma rays in the appropriate region. This simulation shows the gamma rays having a temperature of about 11 MeV, significantly higher than the mean temperature from the FCES results, and more in keeping with the incident hot electron temperature.

Section V: Dosimeter Angular Distribution and Total Gamma Yield

We measured the angular distributions of the daily-cumulative gamma rays by using Landauer Pa area dosimeters placed on the external surface of TC1's tank's wall to measure the dose at ~ 1 m away from the target. The energy response range of

the dosimeters is 5 keV to 40 MeV and a readable dosage range from 1 mrem to 1000 rem. This experiment was carried out during our runs at the Texas Petawatt Laser in 2011, 2012, and 2013. 23 total data sets were collected, but owing to internal instruments obstructing many dosimeter directions on some shots, only 20 sets were usable. These included 4 data sets where platinum targets were used instead of gold, 4 where a mix of platinum and gold targets were used, and 5 sets where differing target shapes such as long thin rods, targets with conic tips, and targets with concave or slant surfaces were used. We exclude the platinum sets in our discussion since there are not enough of them to examine collectively, and we also exclude the mixed sets since the effects of this mix are not easily determined. Different data sets had different angles between laser forward direction and target normal direction, and each data set is the accumulated dosage of between 2 and 8 laser shots.

The angular distributions were fitted to Gaussian distributions and then integrated over the sphere to obtain a total dose, which was then converted into a total gamma energy. We also account for the attenuation from the chamber walls (~1 cm of steel) to obtain a total emergent gamma energy. We accounted for the attenuation by using the simulated spectrum and NIST attenuation data [24]. The results are compiled in Table 2. The conversion efficiency from incident laser energy to gamma rays for the 100 J laser configuration varies from 0.94% to 3.8%, with a mean efficiency of around 2 %. The two days with efficiencies in excess of 3% used targets that were not flat disks or rods. Specifically, they used a combination of “lense” targets, where the back of the target (opposite the laser incidence) and “slant rod” targets, where the surface of the rod facing laser incidence was slanted such that the length of the rod could run down the direction of the laser without reflected laser light damaging the laser apparatus.

Figure 10 shows the gamma-ray yield for gold targets versus laser fluence and versus laser energy. While there is only a slight positive correlation between laser fluence and yield, there is a roughly quadratic relationship between laser energy and gamma ray yield. There is one significant deviation from the trend in laser energy, which corresponds to a dosimeter set when the laser energy was pushed beyond its recommended safety tolerances on the first shot of the day, which may have affected beam quality throughout the day.

Hatchett et al. [25] measured a mean total x-ray energy of 11 J from the Petawatt laser at Lawrence Livermore National Laboratory, whose energy varied from 150-750 J, averaging around 375 J, with an intensity of 3×10^{20} W/cm² on average, incident on 50 – 125 micron thick gold targets. This gives a mean conversion efficiency of about 3%, comparing favorably

with our results. The conversion efficiency of the 50 J laser (the shots in 2011) to gamma rays was only 0.78%.

Figure 11 shows several angular distribution results, while figure 12 shows similar results in polar form. The Full Width, Half Maximum (FWHM) of the Gaussian distribution was about 17° for laser energies of around 45 J, while for more typical energies of ~ 100 J - 120 J the FWHM ranged from 25° to 55° , with a mean of 37° . This compares favorably with the results obtained by Norreys et al of 35° . [26] GEANT4 simulation shows a FWHM of 13° (figure 13), but this is using an incident electron distribution with a FWHM of 20° . This was based on the measured electron distribution of the 50 J configuration of TPW, and indeed the simulated gamma-ray angular distribution is very close to that measured for that laser configuration. The broader distribution for 2012 indicatew that the electron distribution for the 100 J laser was much broader, with a FWHM sometimes exceeding 40° . While it is not clear from the figures, Table 2 shows that the mean angle between the peak of the gamma-ray distribution and the target normal was 26° , towards laser forward, which is close to the PIC simulation results of Sheng et al. [27] of 30° for gamma rays of energies between 0.5 and 30 MeV.

Section VI: Conclusions

For a petawatt class laser irradiating millimeter-thick gold targets, we were able to characterize the gamma-ray spectrum from 3 MeV to 90 MeV using a Forward Compton Electron Spectrometer, with an energy resolution of 0.5 MeV and mean kT of ~ 6 MeV.. We were able to characterize the spectrum from 1 to 7 MeV using a Filter Stack Spectrometer, measuring a mean gamma-ray temperature for the spectrum from 3 to 7 MeV as 2.1 MeV. Dosimeter results show a mean conversion efficiency from laser energy to gamma rays of around 2%, a mean angle between the peak of the gamma distribution and target normal of 26° , and a FWHM of the gamma distribution of 37° .

GEANT4 Monte-Carlo simulation has proven to be adequate for describing the gamma-ray angular distribution and spectrum as well as deconvolving and testing the results from a Forward Compton Electron Spectrometer. In the future we intend to couple this simulation with a PIC code to get an accurate representation of the incident hot electron spectrum and angular distribution and thus to describe the center of the gamma-ray angular distribution with respect to target normal and laser forward.

In addition, we hope to extend the range of the spectrum measured for both the FSS and FCES using more detailed

simulation and careful background subtraction, as well as different strengths and lengths of magnets for the FCES. We also plan to make further use of dosimeters and simulation to characterize and predict the gamma-ray angular distribution and flux. Once these techniques have been refined, we hope to apply them to measuring the spectra of medical x-ray cancer treatment devices.

We also plan to test, through both simulation and experimentation, ways to optimize the gamma-ray yield and angular distribution and ways of using these gamma rays to interrogate shielded nuclear materials.

Bibliography

- [1] E. Liang, S. Wilks, M. Tabak, *Physical Review Letters* 81, 4887 (1998).
- [2] S. C. Wilks, W. L. Kruer, M. Tabak, and A. B. Langdon. *Physical Review Letters*. 69 (9), 1383-1386 (1992).
- [3] Donald Umstadter. *Phys. Plasmas* 8, 1774 (2001).
- [4] P. Gibbon and E. Förster. *Plasma Phys. Control. Fusion* 38, 769 (1996).
- [5] P. Gibbon, *Short Pulse Interactions with Matter: An Introduction* (Imperial College Press, London, 2005).
- [6] Stephen P. Hatchett, Curtis G. Brown, Thomas E. Cowan, Eugene A. Henry, Joy S. Johnson, Michael H. Key, Jeffrey A. Koch, A. Bruce Langdon, Barbara F. Lasinski, Richard W. Lee, Andrew J. Mackinnon, Deanna M. Pennington, Michael D. Perry, Thomas W. Phillips, Markus Roth, T. Craig Sangster, Mike S. Singh, Richard A. Snavely, Mark A. Stoyer, Scott C. Wilks, and Kazuhito Yasuike. *Physics of Plasmas* 7, 2076 (2000)
- [7] W. Heitler, *The Quantum Theory of Radiation*, 3rd Edition (Oxford University Press, London 1954) p. 265.
- [8] Hui Chen, Scott C. Wilks, James D. Bonlie, Edison P. Liang, Jason Myatt, Dwight F. Price, David D. Meyerhofer, and Peter Beiersdorfer. *Physical Review Letters*. 102, 105001 (2009).
- [9] J. Ahrens, H. Borchert, A. Zieger and B. Ziegler. *Nuclear Instruments and Methods* 108. 517-523 (1973).
- [10] Georg Matscheko and Roland Ribberfors. *Phys. Med. Biol.* 32, 5 (1987).
- [11] George L. Morgan, Nicholas S.P. Ring, Paul W. Lisowski, Kefneth G. Boyer, Harald A. Enge, Stanley B. Kowalski, Ronald F. Holsinger, Rober R. Lown, Steve G. Iversen, James R. Tinsley, and Rose Mary Baltrusaitis. *Nuclear Instruments and Methods in Physics Research A* 308, 544-556 (1991).
- [12] Nils Reims, Frank Sukowski, and Kemalettin Kilcarslan. 2012 IEEE Nuclear Science Symposium and Medical Imaging Conference Record (NSS/MIC), M16-66.
- [13] Agostinelli S *et al* 2003 GEANT4—a simulation toolkit *Nucl. Instrum. Meth. A* 506 250–303
- [14] Allison J *et al* 2006 GEANT4 developments and applications *IEEE Trans. Nucl. Sci.* 53 270-8.
- [15] Hui Chen, S. C. Wilks, D. D. Meyerhofer, J. Bonlie, C. D. Chen, S. N. Chen, C. Courtois, L. Elbertson, G. Gregori, W. Kruer, O. Landoas, J. Mithen, J. Myatt, C. D. Murphy, P. Nilson, D. Price, M. Schneider, R. Shepherd, C. Stoeckl, M. Tabak, R. Tommasini, and P. Beiersdorfer. *Physical Review Letters*, 105, 015003 (2010).
- [16] C. D. Chen, J. A. King, M. H. Key, K. U. Akli, F. N. Beg, H. Chen, R. R. Freeman, A. Link, A. J. Mackinnon, A. G. MacPhee, P. K. Patel, M. Porkolab, R. B. Stephens, and L. D. Van Woerkom. *The Review of scientific instruments*, 79(10), 10E305. (2008).
- [17] G. Battistoni, S. Muraro, P.R. Sala, F. Cerutti, A. Ferrari, S. Roesler, A. Fasso`, J. Ranft, *Proceedings of the Hadronic Shower Simulation Workshop 2006, Fermilab 6--8 September 2006*, M. Albrow, R. Raja eds., AIP Conference Proceeding 896, 31-49, (2007)
- [18] A. Ferrari, P.R. Sala, A. Fasso`, and J. Ranft, CERN-2005-10, INFN/TC_05/11, SLAC-R-773 (2005).

- [19] Manfred Matzke. Germany: Physikalisch-Technische Bundesanstalt. (2002).
- [20] M. Reginatto. Physikalisch-Technische Bundesanstalt (PTB), Braunschweig, Germany. (March 1, 2004)
- [21] George B. Rybicki and Alan P Lightman. *Radiative Processes In Astrophysics* (John Wiley and Sons, Inc., New York 1979) p. 198.
- [22] Devin Taylor, Edison Liang, Taylor Clarke, Alexander Henderson, Petr Chaguine, Xin Wang, Gilliss Dyer, Kristina Serratto, Nathan Riley, Michael Donovan, Todd Ditmire. *High Energy Density Physics* 9, 363-368 (2013).
- [23] Alexander Henderson, Edison Liang, Pablo Yepes, Hui Chen, Scott Wilks. *Astrophysics and Space Science* 336, 273-277 (2011).
- [24] National Institute of Standards and Technology. XCOM: Photon Cross Sections Database. <http://www.nist.gov/pml/data/xcom/>. Last accessed 14 November 2013.
- [25] Stephen P. Hatchett, Curtis G. Brown, Thomas E. Cowan, Eugene A. Henry, Joy S. Johnson, Michael H. Key, Jeffrey A. Koch, A. Bruce Langdon, Barbara F. Lasinski, Richard W. Lee, Andrew J. Mackinnon, Deanna M. Pennington, Michael D. Perry, Thomas W. Phillips, Markus Roth, T. Craig Sangster, Mike S. Singh, Richard A. Snavely, Mark A. Stoyer, Scott C. Wilks, and Kazuhito Yasuike. *Physics of Plasmas* 7, 2076 (2000).
- [26] P. A. Norreys, M. Santala, E. Clark, M. Zepf, I. Watts, F. N. Beg, K. Krushelnick, M. Tatarakis, A. E. Dangor, X. Fang, P. Graham, T. McCanny, R. P. Singhal, K. W. D. Ledingham, A. Creswell, D. C. W. Sanderson, J. Magill, A. Machacek, J. S. Wark, R. Allott, B. Kennedy, and D. Neely. *Physics of Plasmas* 6, 2150 (1999).
- [27] Z. M. Sheng, Y. Sentoku, K. Mima, J. Zhang, W. Yu, and J. Meyer-ter-Vehn. *Physical Review Letters* 85, 25 (2000).

Figure Captions:

Figure 1: Diagram of Target Chamber 1 at the Texas Petawatt laser (not to scale). The radius of TC1 was 1 meter. The diagram shows sample positions of the Filter Stack Spectrometer (FSS) and magnetic spectrometers, and the position of the Forward Compton Electron Spectrometer (FCES). When the FCES was in use, the FSS and magnetic spectrometer along its line of sight were moved to a slightly wider angle.

Figure 2a: Electron energy spectrum used for GEANT4 simulation input. The spectrum is the measured output spectrum for a 1 mm gold target shot on the Texas Petawatt Laser.

Figure 2b: Electron angular distribution used for GEANT4 simulation. The Full Width Half Maximum is approximated from dosimeter data from Texas Petawatt Laser experiments.

Figure 3: Filter Stack Spectrometer (FSS) diagram showing type, placement, and thickness of materials.

Figure 4: Filter Stack Spectrometer results from calibrating against a known x-ray source. The approximately known source spectrum is represented by circles and the measured spectrum is represented by triangles.

Figure 5a: Figure 5a: Filter Stack Spectrometer (FSS) results from the Texas Petawatt Laser. The red (solid) line is FSS data and the blue (jagged) line is GEANT4 Monte-Carlo simulation. The target thickness was 1 mm, the laser energy on the target was 100 J and the intensity was $4.3 \times 10^{20} \text{ W/cm}^2$.

Figure 5b: Figure 5b: Filter Stack Spectrometer (FSS) results from the Texas Petawatt Laser. The red (solid) line is FSS data and the blue (jagged) line is GEANT4 Monte-Carlo simulation. The target thickness was 2 mm, the laser energy on the target was 114 J and the intensity was $7.5 \times 10^{20} \text{ W/cm}^2$.

Figure 5c: Figure 5c: Filter Stack Spectrometer (FSS) results from the Texas Petawatt Laser. The red (solid) line is FSS data and the blue (jagged) line is GEANT4 Monte-Carlo simulation. The target thickness was 1 mm, the laser energy on the target was 103 J and the intensity was $3.57 \times 10^{20} \text{ W/cm}^2$.

Figure 6a: Filter Stack Spectrometer tail from the Texas Petawatt Laser. The target thickness was 0.5 mm, the laser energy on the target was 102 J and the intensity was $3.96 \times 10^{20} \text{ W/cm}^2$.

Figure 6b: Filter Stack Spectrometer tail from the Texas Petawatt Laser. The target thickness was 1 mm, the laser energy

on the target was 100 J and the intensity was 4.3×10^{20} W/cm².

Figure 6c: Filter Stack Spectrometer tail from the Texas Petawatt Laser seen in Figure 6b, with the corresponding results from a GEANT4 Monte-Carlo simulation overlaid (jagged line).

Figure 6d: Laser energy versus temperature for the Filter Stack Spectrometer, showing a rough inverse correlation.

Figure 6e: Laser intensity versus temperature for the Filter Stack Spectrometer, showing no obvious correlation.

Figure 7: Forward Compton Electron Spectrometer (FCES) diagram, side view.

Figure 8: Flow-chart demonstrating the process for turning an image plate read-out into a gamma-ray spectrum.

Figure 9a: Comparison between Forward Compton Electron Spectrometer (FCES) deconvolved spectrum (red) and simulation (blue). The FCES used a converter consisting of 12.5 mm plastic followed by 7 mm of copper. A teflon collimator was used to reduce the acceptance angle to 5.5 degrees.

Figure 9b: Comparison between Forward Compton Electron Spectrometer (FCES) deconvolved spectrum (red) and simulation (blue). The FCES used a converter consisting of 12.5 mm plastic followed by 7 mm of tin. A teflon collimator was used to reduce the acceptance angle to 5.5 degrees.

Figure 9c: Comparison between Forward Compton Electron Spectrometer (FCES) deconvolved spectrum (red) and simulation (blue). The FCES used a converter consisting of 12.5 mm plastic followed by 7 mm of copper. A teflon collimator was used to reduce the acceptance angle to 11.5 degrees.

Figure 9d: Measurement of the slope of the gamma ray spectrum in GEANT4 simulation. Only the energy range 6-50 MeV is considered, in keeping with the limitations of the FCES. The target used was a 1 mm thick gold target, and the electron spectrum was as seen in figure 2.

Figure 10a: Dosimeter results for gold targets showing laser fluence versus efficiency. While the 2011 data, with an average fluence below 10^{20} W/cm², does show a lower efficiency than the data sets with fluences at least a few times 10^{20} W/cm², the efficiency is nearly flat in fluence otherwise.

Figure 10b: Dosimeter results for gold targets showing laser energy versus efficiency. The efficiency increases roughly exponentially, except for one point below 1% efficiency but above 110 J of laser energy, where the laser was pushed past its recommended safety tolerances, which may have affected the beam quality.

Figure 11a: Dosimeter results for 2012, day 5, which had 4 lasers shots with energy of about 100 J each. All targets were gold.

Figure 11b: Dosimeter results for 2012, day 6, which had 5 lasers shots with energy of about 100 J each. All targets were gold.

Figure 11c: Dosimeter results for 2013, day 7, which had 7 lasers shots with energy of about 108 J each. All targets were gold targets with thicknesses much greater than the target diameter ("rod targets").

Figure 11d: Dosimeter results for 2013, day 3, which consisted entirely of platinum targets. There were 3 shots which had about 100 J of energy each.

Figure 11e: Dosimeter results for 2013, day 10, which had 6 lasers shots with energy of about 120 J each. Targets were a mix of gold and platinum.

Figure 12a: Dosimeter polar plot for 2012, day 5, which had 4 lasers shots with energy of about 100 J each. All targets were gold.

Figure 12b: Dosimeter polar plot for 2012, day 6, which had 5 lasers shots with energy of about 100 J each. All targets

were gold.

Figure 12c: Dosimeter polar plot for 2013, day 7, which had 7 lasers shots with energy of about 108 J each. All targets were gold targets with thicknesses much greater than the target diameter (“rod targets”).

Figure 12d: Dosimeter polar plot for 2013, day 3, which consisted entirely of platinum targets. There were 3 shots which had about 100 J of energy each.

Figure 12e: Dosimeter polar plot for 2013, day 10, which had 6 lasers shots with energy of about 120 J each. Targets were a mix of gold and platinum.

Figure 13: Gamma-ray angular distribution from GEANT4 simulation, using a 20 degree Full-Width-Half-Maximum electron distribution. The relative lack of gamma rays near 0 degrees results from gamma rays being produced by the scattering of relativistic electrons, resulting in the gamma rays having small but non-zero deflection.

Year	2011	2012	2013
Total Laser Energy (J)	37.1 - 48.4	82 - 130	86 - 129
Pulse Duration (fs)	182-433	141 - 245	120-352
Peak Laser Power (TW)	Not Available	450 - 802	326-899
Peak Laser Intensity (W/cm ²)	$1.6 \cdot 10^{19} - 2 \cdot 10^{20}$	$2.83 \cdot 10^{20} - 1.85 \cdot 10^{21}$	$1.9 \cdot 10^{20} - 1.1 \cdot 10^{21}$
Mean Laser Energy (J)	43.8	98	109
Mean Pulse Duration (fs)	330	169	160
Mean Peak Laser Power (TW)	Not Available	585	689
Mean Peak Laser Intensity (W/cm ²)	$1.0 \cdot 10^{20}$	$8.3 \cdot 10^{20}$	$5.4 \cdot 10^{20}$

Table 1: Texas Petawatt Laser (TPW) parameters. A major upgrade was performed on the TPW between 2011 and 2012.

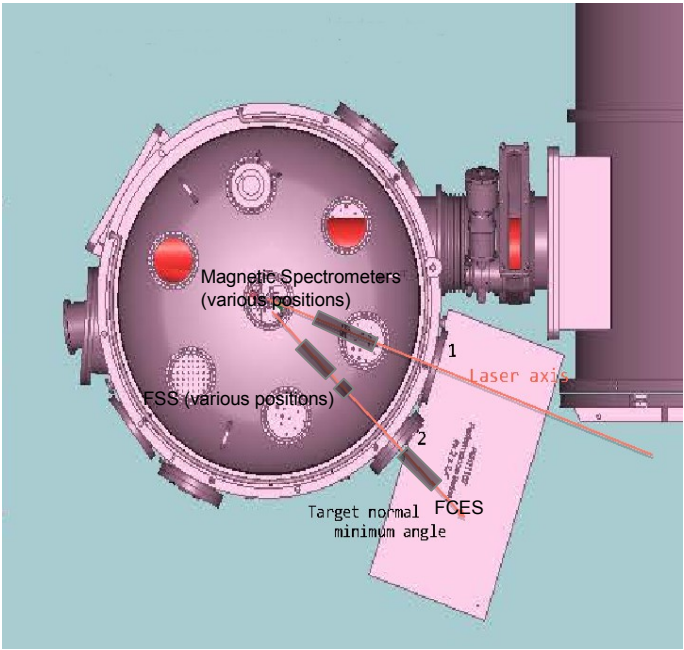
Year, Day	Total Laser Energy (J)	Total Gamma Energy (J)	Number of Shots	Angle between target normal and laser forward (Degrees)	Angle Between Target Normal And Peak of Gamma Distribution (Degrees)	FWHM of Gamma Distribution (Degrees)	Efficiency (%)	Target Type
2011	219	1.70	5	25	10	17	0.78	Au
2012, 1	477	43.4	5	25	35	34	1.4	Au
2012, 2	341	3.19	3	25	21	33	0.93	Au
2012, 5	404	10.5	4	35	31	34	1.9	Au
2012, 6	510	9.36	5	45	25	26	2.1	Au
2012, 7	602	8.54	6	40	21	25	1.5	Au
2012, 8	786	6.96	6	40	24	25	1.6	Au
2012, 10	730.7	8.44	8	35	29	37	1.4	Au
2013, 1	198	2.94	2	25	25	33	0.63	Pt
2013, 2	398	0.388	4	25	36	45	0.097	Pt
2013, 3	283	8.19	3	25	19	38	2.9	Pt
2013, 4	421	8.32	4	25	26	42	2.0	Pt
2013, 5	521	18.2	5	25	18	48	3.8	Au
2013, 6	574	26.5	5	25	15	60	3.7	Au
2013, 7	758	11.1	7	25	28	46	1.5	Au
2013, 8	773	12.4	7	25	27	41	1.6	Au/Pt
2013, 9	866	24.1	7	25	24	29	2.8	Au
2013, 10	722	16.2	6	25	26	29	2.2	Au/Pt
2013, 11	647	9.15	6	25	29	33	1.4	Au/Pt
2013, 12	708	9.28	7	25	27	33	1.3	Au/Pt

Table 2: Summary of dosimeter results. 2 days in 2012 were unusable due to a large number of obstructions inside the chamber.

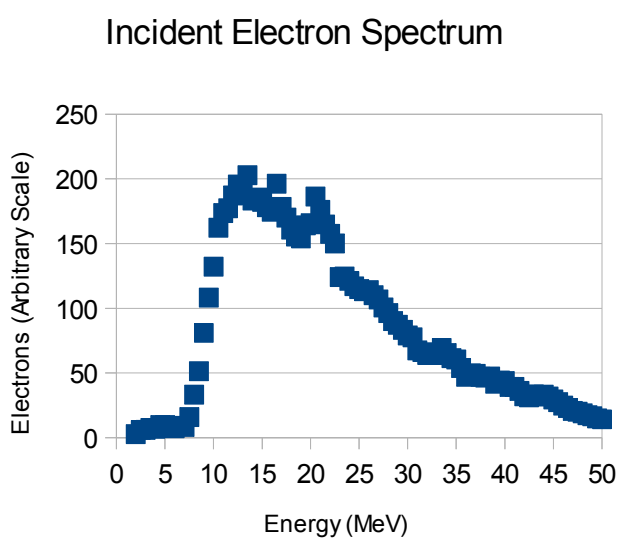
Supplementary material for equations

[Click here to download Supplementary material for on-line publication only: GammaPaperDraft3.pdf](#)

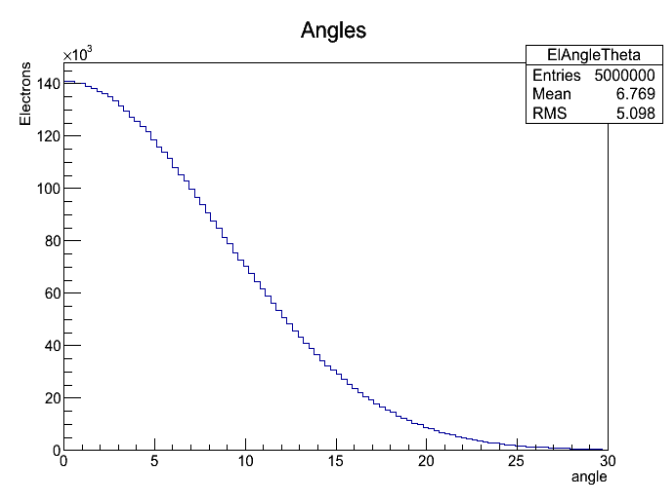
Figure



Figure

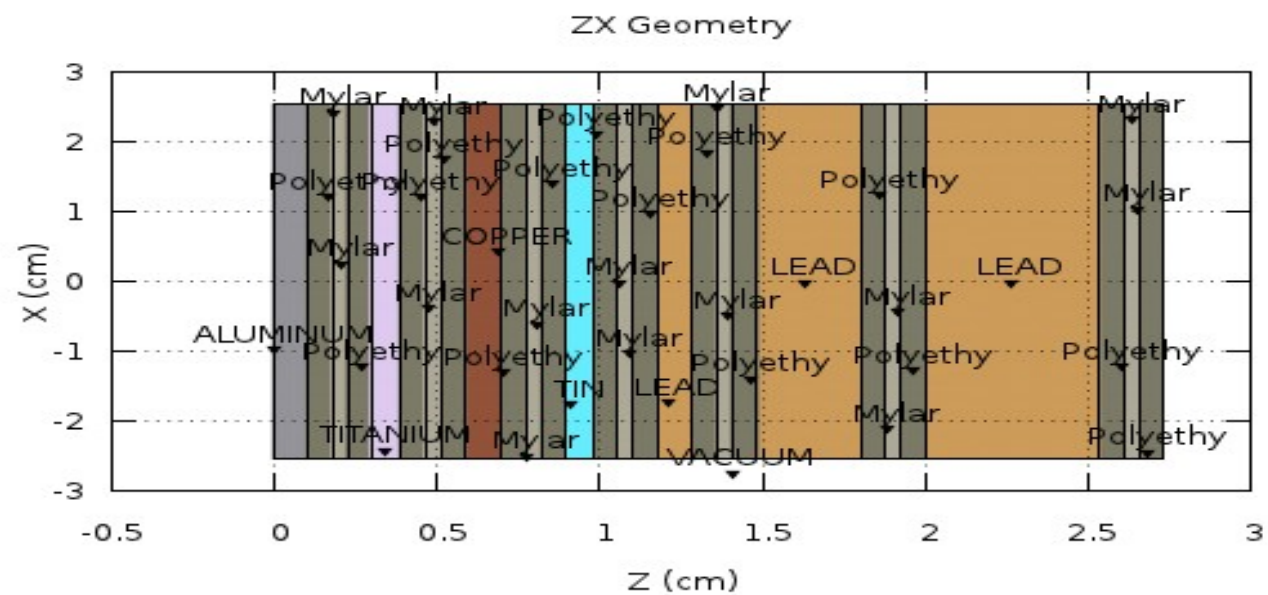


(a)

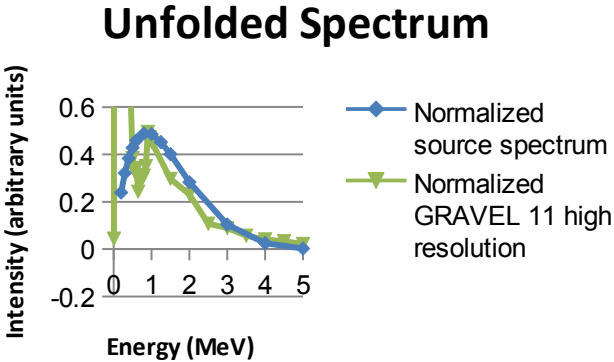


(b)

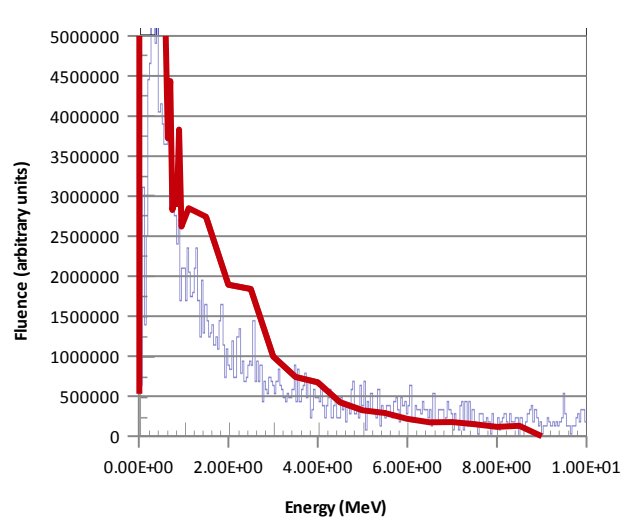
Figure



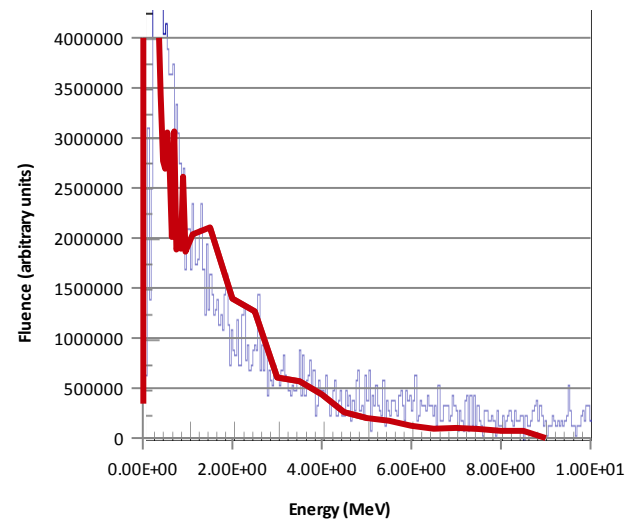
Figure



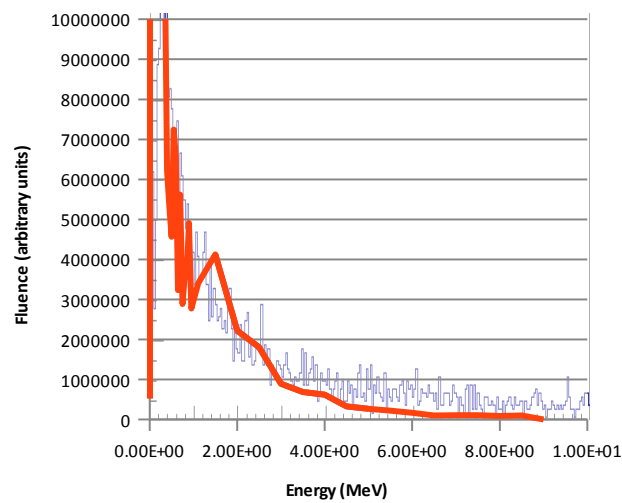
Figure



(a)

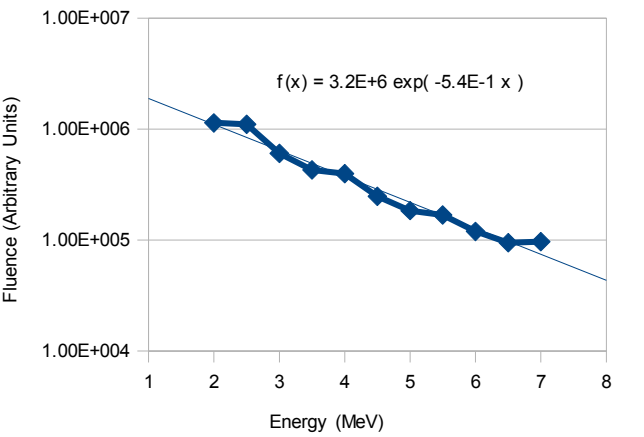


(b)

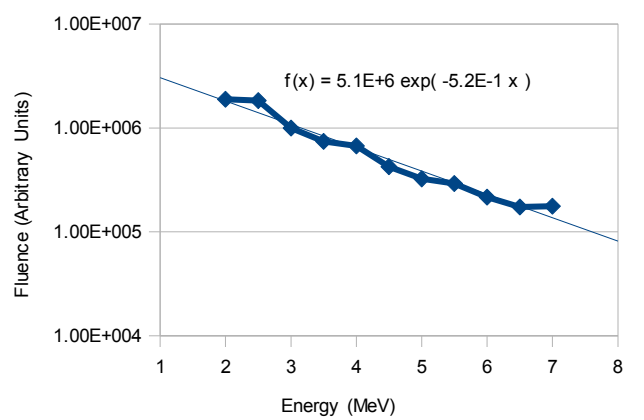


(c)

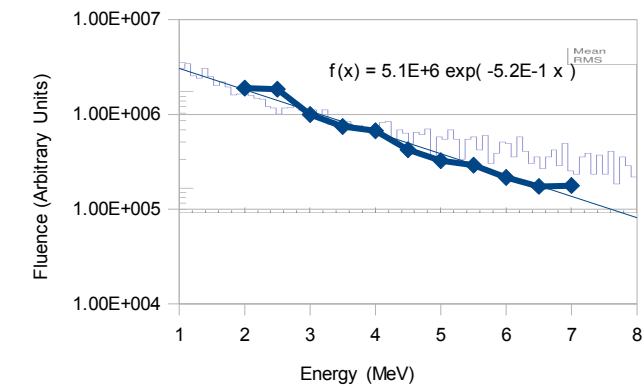
Figure



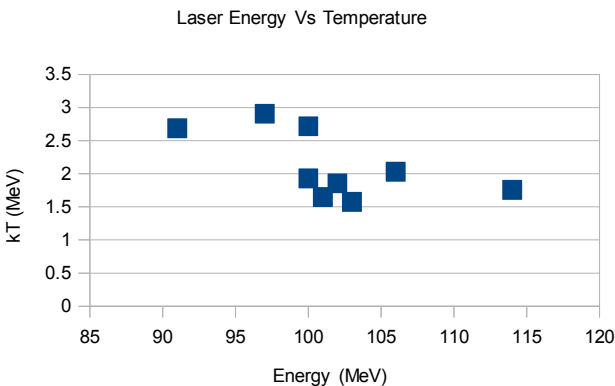
(a)



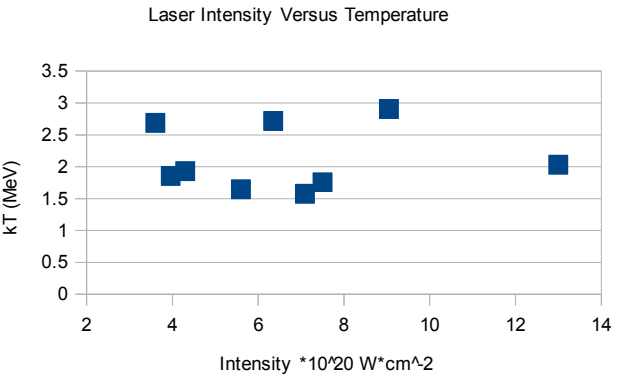
(b)



(c)

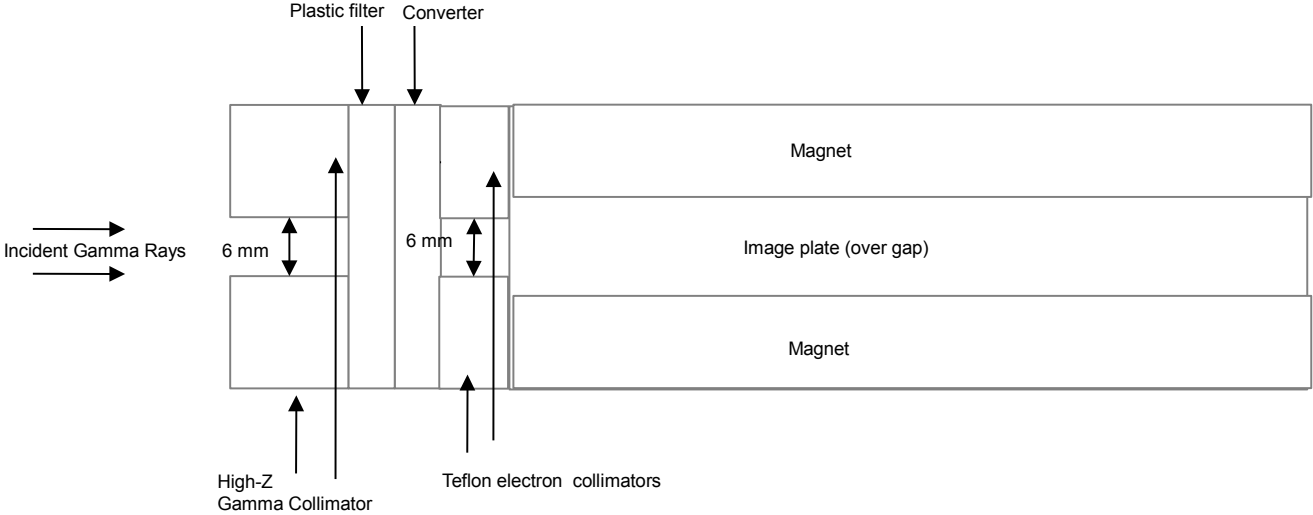


(d)



(e)

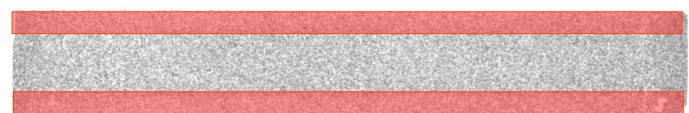
Figure



Figure



e-



e+

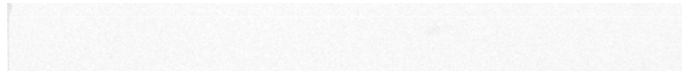
Separate
Background Region
(shaded regions)



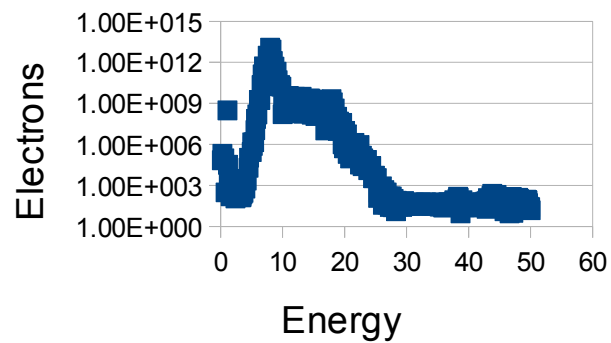
Subtract e+
plate from e-
plate, by region



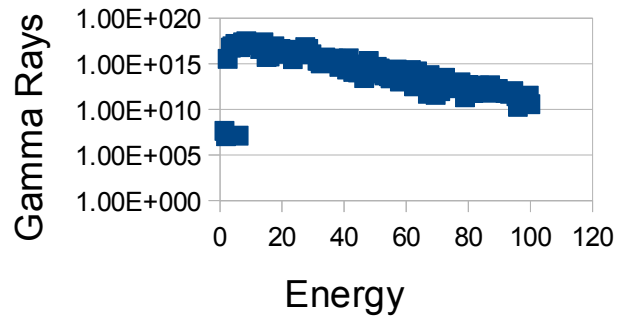
Average
background
region in pixel
columns



Subtract background
from the rest of the
image, by pixel
column

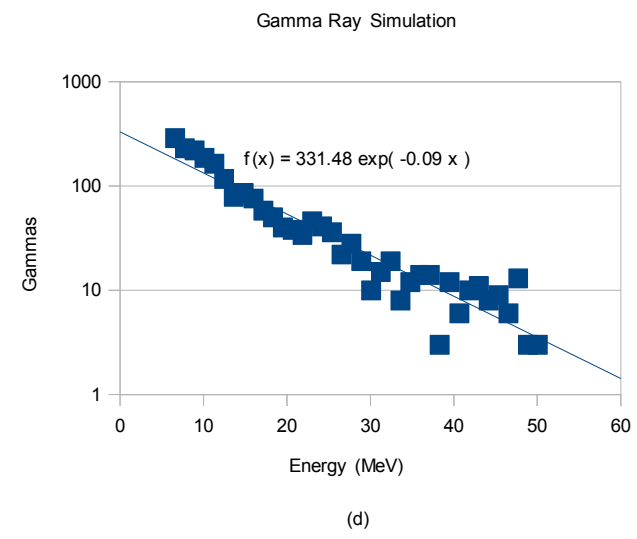
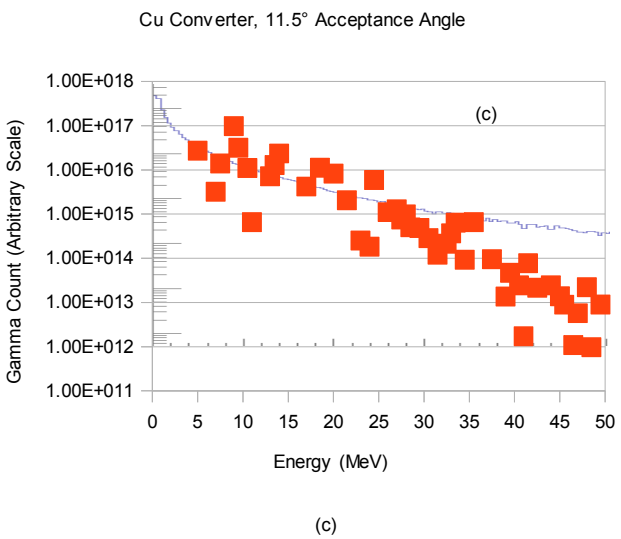
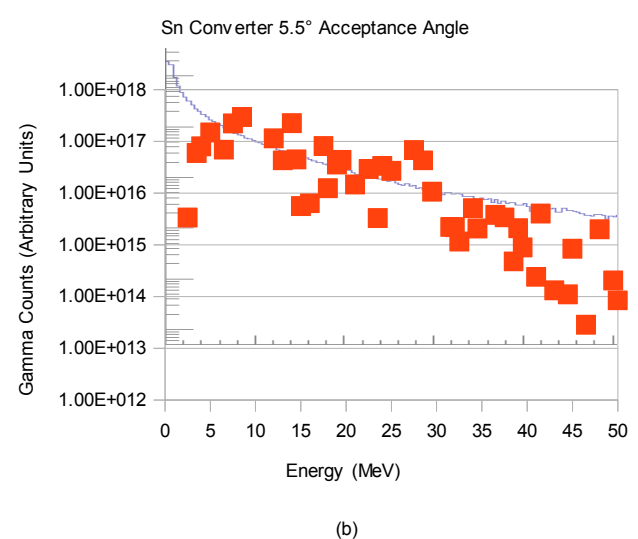
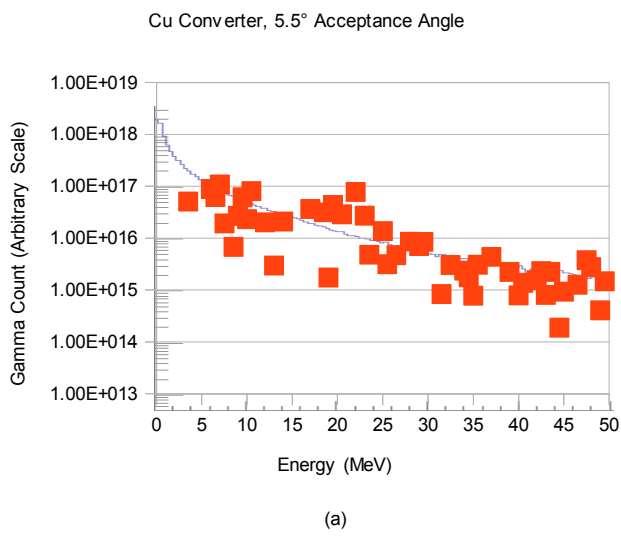


Deconvolve image into Compton
electron spectrum

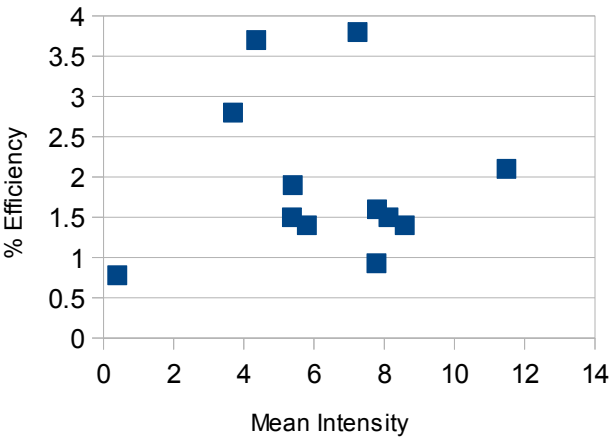


Deconvolve electron spectrum
into gamma-ray spectrum

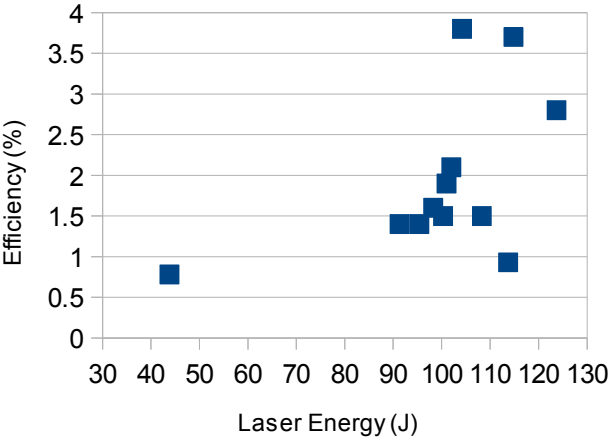
Figure



Figure

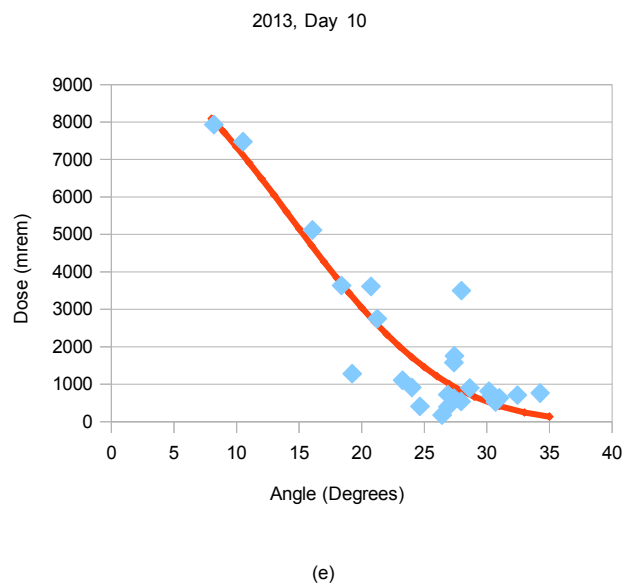
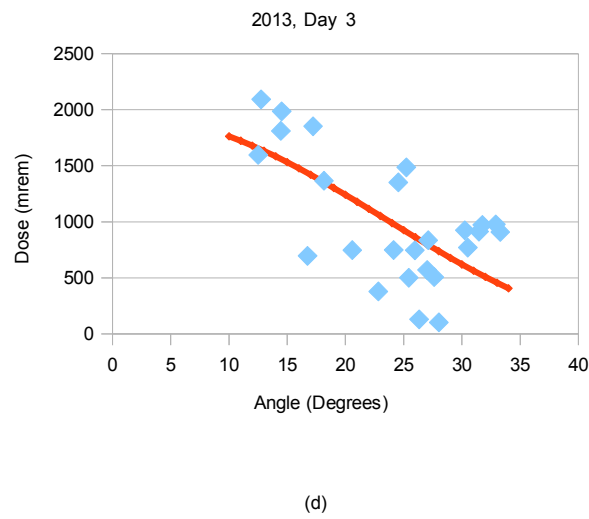
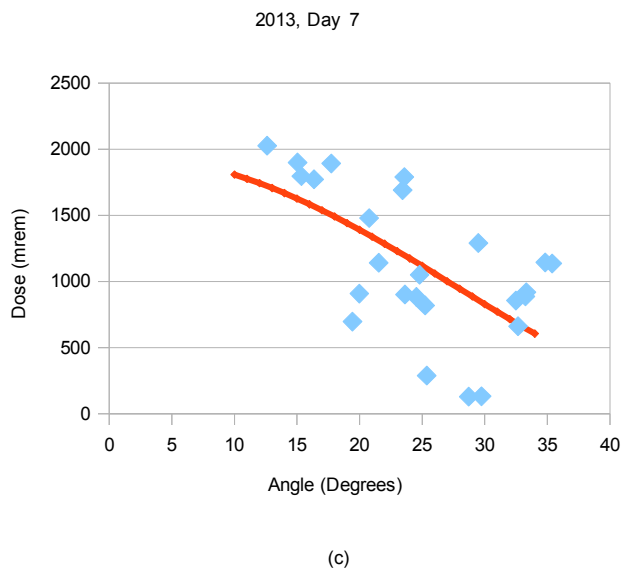
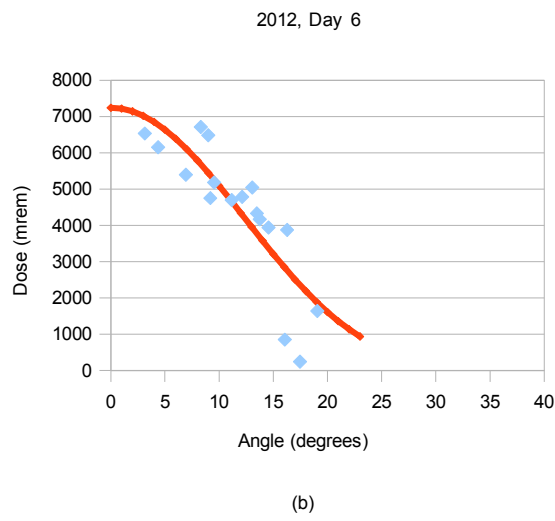
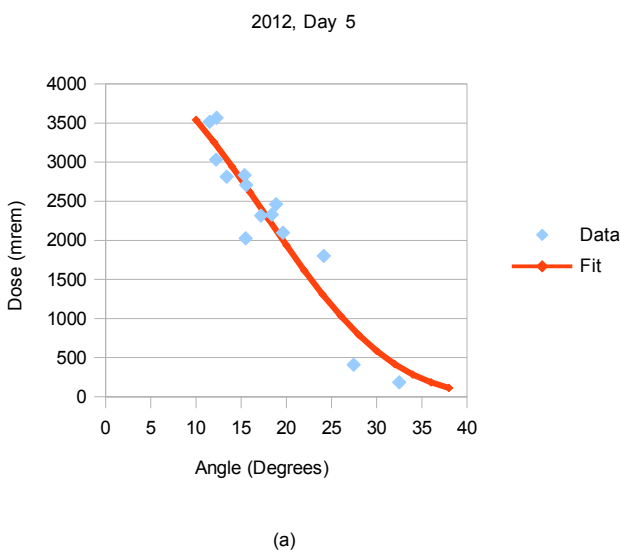


(a)

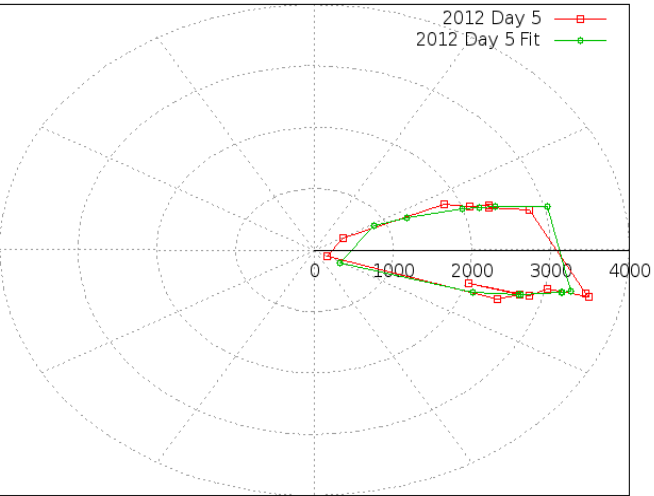


(b)

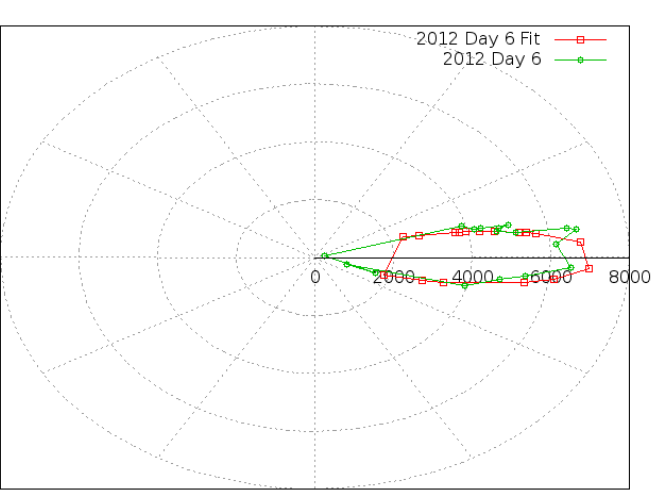
Figure



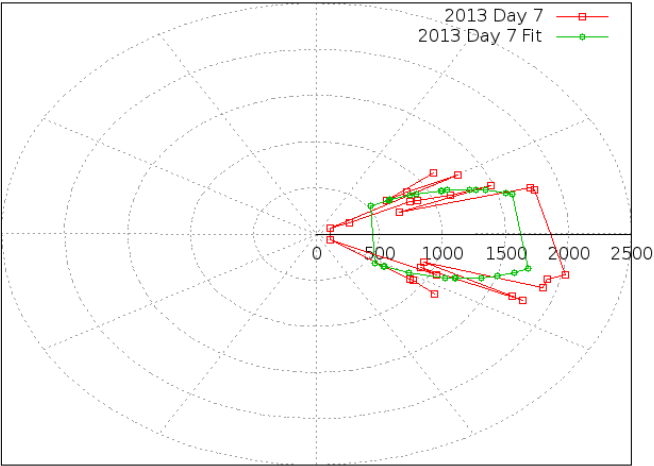
Figure



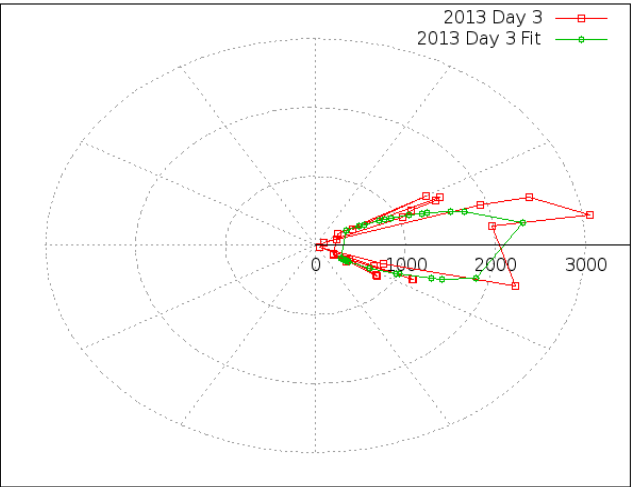
(a)



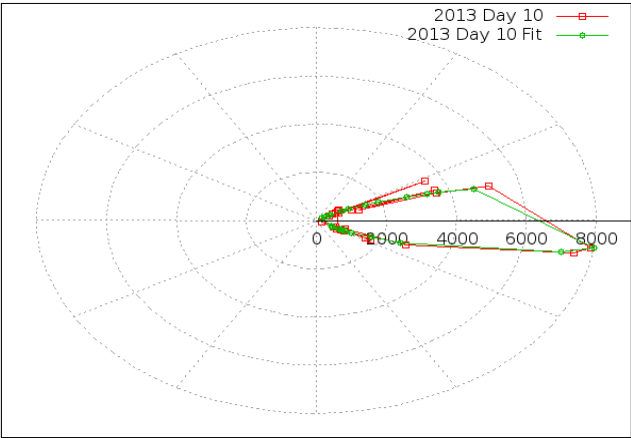
(b)



(c)



(d)



(e)